Asian Journal of Information Technology 6 (3): 303-308, 2007


# Extraction of Structural Shape of Low DOF Image Using Morphological Operators

[1]N. Santhi, [2]Seldev Christopher, [3]K. Ramar and [4]J. Arun Prem Santh
[1]NI College of Engineering, Kumaracoil, India
[2]CSE Institute of Technology, Thovalai, India
[3]Department of CSE, National Engineering College, Kovilpatti, India
[4]ME Communication Systems, NI College of Engineering, Kumaracoil, India

**Abstract:** Automatic image segmentation and shape extraction is one of the most Challenging problems in computer vision.This study presents a novel algorithm to partition an image with low Depth-of-Field (DOF) into focused Object-of-Interest (OOI) and extracts the structural shape components using a generalized discrete morphological skeleton transform.The proposed segmentation algorithm unfolds into three steps. In the first step, we transform the low DOF image into an appropriate feature space, in which the spatial distribution of the high-frequency components is represented. This is conducted by computing Higher Order Statistics (HOS) for all pixels in the low-DOF image. Next, the obtained feature space, which is called HOS map in this study, is simplified by removing small dark holes and bright patches using a morphological filter by reconstruction. Finally, the OOI is extracted by applying region merging to the simplified image and by thresholding. Unlike the previous methods that rely on sharp details of OOI only, the proposed algorithm complements the limitation of them by using morphological filters, which also allows perfect preservation of the contour information. For the morphological shape representation algorithms, a generalized discrete morphological skelton transform is used which uses eight structuring elements to generate skeleton subsets will be adjacent to each other. Each skeletal point will represent a shape part that is in general an octagon with four pairs of parallel opposing sides. The number of representative points needed to represent a given shape is significantly lower than that in the standard skeleton transform. A collection of shape components needed to build a structural representation is easily derived from the generalized skeleton transform. Each shape component covers a significant area of the given shape and severe overlapping is avoided. The given shape can also be accurately approximated using a small number of shape components.

**Key words:** Extraction, structural shape, DOF, morphological, HOS, algorithm

## INTRODUCTION

In this study, our focus is to build an efficient structural shape representation that allows exact as well as approximate reconstructions of the input shapes. Therefore, we are following a structural and algebraic approach to shape representation. In the Morphological Skeleton Transform(MST), a given shape is represented as a union of all maximal disks contained in the shape (Gonzale and Wang *et al*., 1992). There is much overlapping among the maximal disks. The Morphological Shape Decomposition (MSD) is another important morphological shape representation scheme (Wang *et al*., 2001) in which a given shape is represented as a union of certain disks contained in the shape. The overlapping among representative disks of different sizes is eliminated new morphological shape representation algorithm that can be viewed as a compromise between the MST and the MSD was recently proposed (Best and Jain, 1988; Lifshitz and Pizer, 1990). In this scheme, overlapping among representative disks of different sizes is allowed, but severe overlapping among such disks is avoided. We can call this algorithm Overlapped Morphological Shape Decomposition (OMSD). The advantages of these basic algorithms include that they have simple and well-defined mathematical characterizations and they are easy and efficient to implement. There is a common problem shared by all 3 algorithms. In general, there is much overlapping among representative disks of the same size. The MST is not typically considered a shape decomposition algorithm because of the heavy overlapping among the representative disks. For the MSD and OMSD, there is a simple scheme for grouping representative disks into shape components.

In this study, we will develop a generalized discrete skeleton transform. In the new algorithm, the size of a

**Corresponding Author:** N. Santhi, NI College of Engineering, Kumaracoil, India

typical skeleton subset is much smaller. In our new algorithm, each shape element, which is a shape part represented by a representative point, is in general an octagon with four pairs of parallel opposing sides. The two sides in each opposing pair also have the same size. We will also develop a new shape decomposition algorithm based on the new skeleton transform. The use of octagons as shape components also provides some flexibility in describing natural shape parts. Therefore, an accurate approximation of an input shape can often be constructed by using only a very small number of major shape components. The algorithm consists of the following steps:

- Feature space transformation using HOS
- HOS map simplification by Morphological filters
- Region Merging And Adaptive Thresholding
- Extraction of structural shape components

**Feature space transformation using HOS:** The first step toward segmentation consists in transforming the input low-DOF image into an appropriate feature space. The choice of the feature space depends on the applications that the algorithm is aimed at. For instance, the feature space may represent the set of wavelet coefficients or local variance image field (Won *et al*., 2002).

In this project, HOS (Gelle, 1997) for feature space transformation can be computed. HOS are well suited to solving detection and classification problems because they can suppress Gaussian noise and preserve some of the non-Gaussian information in this project, the fourth-order moments are calculated for all pixels in the image.The fourth-order moment at (x, y) is defined as follows:

$$\hat{m}^{(4)}(x,y)=\frac{1}{N_\eta}\sum_{(s,t)\in\eta(x,y)}(I(s,t)-\hat{m}(x,y))^4$$

where $\eta(x,y)$ is a set of neighboring pixels centering at(x,y), m(x,y) is the sample mean of I(x,y)(i.e., (x,y) = $(1/N_\eta)\sum_{(s,t)\in\eta(x,y)}$ I(s,t)) and $N_\eta$ is a size of $\eta$. Since the dynamic range of the fourth-order moment values is extremely large, the value for each pixel is down scaled and limited by 255 such that each pixel takes a value from [0, 255]. The outcome image is called a HOS map. At a pixel(x,y)$\in$R, a component of the HOS map, HOS(x,y), is defined as follows:

$$HOS(x,y)=\min\left(255,\frac{\hat{m}^{(4)}(x,y)}{DSF}\right)$$

Where DSF denotes down scaling factor. For a variety of test images, it is observed that 100 are appropriate for DSF. By applying above equation for all pixels, we have a HOS map, O= {HOS(x, y);(x, y) $\in$R}.. Comparing it to a local variance map, it can be observe that the HOS map yields denser and higher values in the focused areas, suppressing noise in the defocused regions. The strong edges of focused region are calculated by snake algorithm.

**HOS map simplification by morphological filtering by reconstruction:** In the previous study, feature space transformation was addressed such that more adequate feature space is exploited for segmentation. The HOS map transformed from the low-DOF image has gray levels ranging from 0 to 255, where high values indicate the existence of high-frequency components (i.e., possibly focused regions). However, there could be some focused smooth regions, which may not be easily detected by HOS transformation. Similarly, defocused texture regions may generate noise.Therefore, a proper tool for HOS map simplification is needed to remove these errors, appearing in the form of small dark and bright patches in focused and defocused regions, respectively.

The elementary geodesic erosion $\varepsilon^{(1)}(O,O_R)$ of size one of the original image O with respect to the reference image ORis defined as

$$\varepsilon^{(1)}(O,O_R)(x,y)=\max\left\{E_B(O)(x,y),O_R(x,y)\right\}$$

and the geodesic dilation d $\delta^{(1)}(O,O_R)$ of size one of the original image $O_R$ with respect to the reference image OR is defined as

$$\delta^{(1)}(O,O_R)(x,y)=\min\left\{\delta_B(O)(x,y),O_R(x,y)\right\}$$

Thus, the geodesic dilation d $\delta^{(1)}(O,O_R)$ dilates the image O using the classical dilation operator $\delta_B(O)$.As we know, dilated gray values are greater or equal to the original values in O. However, geodesic dilation limits these to the corresponding gray values of $O_R$ . The choice of the reference image will be discussed shortly.

The erosions and dilations of arbitrary size are obtained by iterating the elementary versions $\varepsilon^{(1)}(O,O_R)$ and $\delta^{(1)}(O,O_R)$ accordingly. For example, the geodesic erosion (dilation) of infinite size, which is so-called reconstruction by erosion (by dilation), is given by the following.

- Reconstruction by erosion:

$$\varphi^{(rec)}(O,O_R)=\varepsilon^{(\infty)}(O,O_R)=\varepsilon^{(1)}{}_0\,\varepsilon^{(1)}{}_0\ldots{}_0\varepsilon^{(1)}(O,O_R)$$

- Reconstruction by dilation:

$$\gamma^{(rec)}(O,O_R)=\delta^{(\infty)}(O,O_R)=\delta^{(1)}{}_0\delta^{(1)}{}_0\cdots{}_0\delta^{(1)}(O,O_R).$$

Notice that $\varphi^{(rec)}(O,O_R)$ and $\gamma^{(rec)}(O,O_R)$ will reach stability after a certain number of iterations.

In the proposed system, morphological closing-opening by reconstruction, which is morphological closing by reconstruction followed by morphological opening by reconstruction are employed. The strength of the morphological closing-opening by reconstruction filter is that it fills small dark holes and removes small bright isolated patches, whereas perfectly preserving other components and their contours. Obviously, the size of removed components depends on the size of the structuring element. The focused smooth regions can be well covered whereas the scattered small regions in the background can be removed by the filter.

**Region merging and adaptive thresholding:** In typical morphological segmentation techniques, the simplification by morphological filters is followed by marker extraction and watershed algorithm to partition an image or scene into homogeneous regions in terms of intensity. Unlike the abovementioned conventional intensity-based segmentation schemes, the task of the low-DOF image segmentation is to extract focused region (i.e., OOI)from the image rather than partitioning the image. The decision process consists of two steps: Region merging and final decision by thresholding.

**Region merging:** Region merging is started based on seed regions, which can be regarded as definitely focused regions of OOI. First, every flat zone is treated as a region regardless of its size, which means even one pixel zone can become a region. Then, we define regions having the highest value in the simplified HOS map as seed regions and these seed regions become initial OOI [see white areas in Fig. 1c and a].

We also define regions having values less than or equal to a predefined value $T_L(T_L<v_h$ )as definitely defocused regions. Those regions are labeled as initial $OOI^c$.Then, the remaining regions are labeled as uncertainty regions with pixel values $(T_L,v_h)$. A pictorial example is shown in Fig. 1a, where the initial OOI and OOI are denoted by white and black regions, respectively, whereas the dashed regions $R_i$, $R_j$ and Rkindicate uncertainty regions. Our goal in this region merging process is to assign uncertainty regions to either OOI or $OOI^c$.Such an assignment is iteratively conducted by considering bordering relationship between uncertainty region and current OOI and $OOI_n$ (i.e., OOI at the iteration). Specifically, we develop an algorithm that

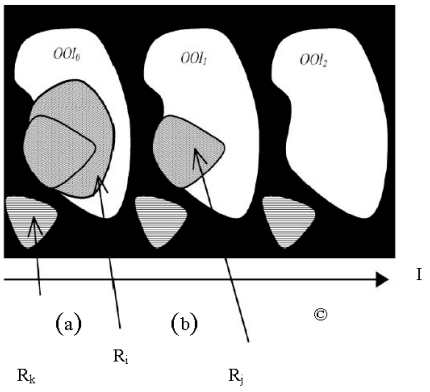


Fig. 1: Evolution of OOI by the proposed region merging. (a) Initial OOI and three uncertain regions with pixel values $(T_L;v_H)$ in the simplified HOS map. (b) R is merged into OOI. (c) Final OOI, after R is merged into OOI

assigns an uncertainty region $R_n$,$i_{in}$ the $n^{th}$iteration to either OOI or $OOI_n^c$ by computing normalized overlapped boundary (nob).

The normalized overlapped boundary can be modeled as a continuous random variable nob, taking values of nob in [0, 1]. If is larger than a threshold value, the region is merged to OOI.Then, the partition is updated, yielding an increasing sequence of OOI which eventually converges to OOI. A reasonable starting point for finding the threshold value, which is denoted by, is to use the likelihood ratio test as follows

$$\text{Assigv } R_i \text{ to } 00I \text{ if } P(00I \mid nob_i) > P(00I^c \mid nob_i), \text{ other wise assign to } 00I^c$$

where OOI represents the class for the OOI with prior probability P(OOI) and $OOI^c$ denotes the class for the non-OOI with prior probability $P(OOI^c)$=1-P(OOI).P(OOI/nobi). and $P(OOI^c$ / nobi) represent the a posteriori conditional probabilities that correspond to H1 and H0, respectively. If we apply Bayes theorem on both sides of the expression and rearrange terms as follows:

$$\frac{p(nob_i \mid OOI)}{p(nob_i \mid OOI^c)} \underset{H_0}{\overset{H_1}{\gtrless}} \frac{P(OOI^c)}{P(OOI)}$$

The left-hand ratio is known as the likelihood ratio and the entire equation is often referred to as the likelihood ratio test. Since the test is based on choosing the region class with maximum a posteriori probability, the

decision criterion is called the Maximum A Posteriori (MAP) criterion. It is also called the minimum error criterion, since on the average; this criterion yields the minimum number of incorrect decisions. Since the OOI and background may have any size and shape, we assume equal priors (P(OOI)= P(OOI$^c$) and thus, the expression reduces to the Maximum Likelihood (ML) criterion

$$\frac{p(nob_i \mid OOI)}{p(nob_i \mid OOI^c)} \underset{H_0}{\overset{H_1}{\gtrless}} 1.$$

We propose to model the class-conditional probability density functions by exponential distributions

$$p(nob_i \mid OOI^c)=\lambda_{1e}\, e^{-\lambda_1 nob_i}\, u(nob_i)$$
$$p(nob_i \mid OOI)=\lambda_{2e}\, e^{-\lambda 2(1-nob_i)}\, u(nob_i)$$

where u(x) denotes the step function. We believe that these distributions are suited to the real data because p(nob$_i$ / OOI) would have high values around nob$_i$ =1 and rapidly decay as nob$_i$→0, whereas p(nob$_i$/OOI$^c$)would have high values around nob$_i$ =0 and rapidly decay as nob$_i$→1. Finally, optimal threshold for can be obtained as

$$nob_{i<H0}^{>H1} \frac{\lambda_2}{\lambda_1+\lambda_2}+\frac{In\left(\frac{\lambda_1}{\lambda_2}\right)}{\lambda_1+\lambda_2}=T_{nob}$$

The parameters $\lambda_1$and $\lambda_2$can be estimated from the actual data. However, if we assume symmetry between the exponential distributions ($\lambda_1$=$\lambda_2$), the expression for the optimal threshold can be approximated and simplified as

$$T_{nob}=\frac{\lambda_2}{\lambda_1+\lambda_2}+\frac{In\left(\frac{\lambda_1}{\lambda_2}\right)}{\lambda_1+\lambda_2}\approx\frac{1}{2}$$

Hence, if nob$_i$ is larger than T$_{nob}$, R$_i$ is merged to OOI and OOI is updated. This process is iterated until no merging occurs. A pictorial illustration is provided in Fig. 1. In Fig. 1a, nob$_i$ is greater than T$_{nob}$, thus Rimerges into OOI, whereas Rk does not since nobk is less than T$_{nob}$. In the next iteration, as shown in Fig. 1b, R$_j$ merges into OOI since nob$_j$> T$_{nob}$. In order to expedite the process, very small regions can be merged to the neighbor region with nearest value in advance.

**Final decision:** In the preceding subsection, the focused regions (i.e., OOI) are updated by region merging. In other words, an uncertainty region whose nob is larger than T$_{nob}$, has been incorporated into OOI. Now, the final decision becomes to extract OOI from the final Partition P. It is easily done by extracting regions having the highest value. For instance, in Fig. 1(c), OOI will be extracted whereas Rk will not be decided as OOI since it has a value than less than that of OOI.

**Extraction of structural shape components:** In traditional skeleton transform shape will be represented as a union of maximal line segments since it uses single line segment as structuring element, In our algorithm, we will use multiple structuring elements that are line segments with different orientations. Another strategy used by our algorithm is to apply skeleton transform steps with one structuring element to skeleton subsets obtained using other structuring elements.

**New algorithm:** In our algorithm, we use eight basic structuring elements B$_0$,B$_1$ …B$_7$ as shown in Fig. 2. In fact B $_4$, B$_5$, B$_6$ and B$_7$are translated versions of B $_0$, B$_1$, B$_2$ and B$_3$, respectively. We use all eight structuring elements in order for our final shape elements to be as symmetric as possible. In our new algorithm, we obtain the skeleton subsets by repeatedly applying erosion operations using these eight structuring elements in the following order: B$_0$,B$_1$…B$_7$, B$_0$, B $_1$..B $_,_7$B $_,_0$B $_._1$. That is, these eight structuring elements will be applied in a cyclic sequence. A given shape image is a set of points. Our algorithm can be viewed as a recursive process of applying erosion operations to repeatedly reduce a set into two smaller sets.For a nonempty image X that is not a set of isolated points, let

$$Y_0 (X) = X \Theta B0$$
$$Z0 (X)=X \setminus (Y_0 (X) \oplus B0)=X \setminus (X \circ B_0)$$

In general, X is reduced to two smaller sets Y0 (X) and Z0 (X) by this erosion step the final shape elements represented by the points in the skeletons subsets are maximal shape elements in the sense that they cannot be expanded any further following the sequence of expansion steps used in the algorithm. The union of all the final shape elements is the given shape X. Each final shape element is in general an octagon with four pairs of

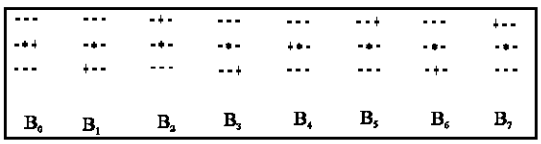


Fig. 2: Eight basic structuring elements

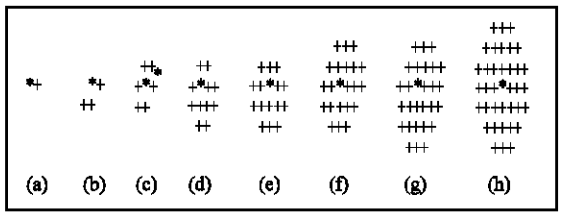


Fig. 3: Shape elements generated using basic structuring elements

parallel opposing sides. The two sides in each opposing pair also have the same length. Some of these octagons are shown in Fig. 3. Figure 3a-h show following eight shape elements: $B_0$, $B_0 \oplus B_1$, $B_0 \oplus B_1 \oplus B_2$... $B_0 \oplus B_1 \oplus \ldots \oplus B_7$. There is a simple relationship between the shape of a shape element and the numbers of different structuring elements used. The number of $B_0$ or $B_4$ used to construct a shape element equals the size of the shape element's two horizontal sides.The number of $B_2$or $B_6$used is same as the size of two vertical sides. The numbers of other two pairs of structuring elements used determine the sizes of two pairs of diagonal sides.

The number of $B_0$ or $B_4$ used to construct a shape element equals the size of the shape element equals the size of shape elements two horizontal sides. The number of $B_2$ or $B_6$ used is same as the size of two vertical sides. The numbers of other two pairs of structuring elements used determine the sizes of two pairs of diagonal sides.

In our generalized skeleton algorithm, a given shape is represented as a union of all generalized maximal "disks" contained in the shape. We eliminated the heavy overlapping among representative shape elements of the same shape and size.

However, there can still be much overlapping among representative shape elements of different shapes and sizes. The generalized skeleton transform makes the derivation of this shape decomposition and the selections of its shape components very easy. In this new algorithm, the generalized skeleton transform allows us to easily select a single point to represent a shape component covering a new area in a given shape.

## CONCLUSION

This algorithm separates the pixels in the low-DOF images into two regions based on their higher order statistics. To this end, the low-DOF image was transformed into an appropriate feature space, which was called HOS map in this study. Morphological filter by reconstruction was applied to simplify the HOS map, followed by region-merging technique and thresholding for final decision. By employing the powerful morphological tool for simplification, the proposed scheme performs well even for focused smooth regions as far as their boundaries contain high frequency components (i.e., edges).Also, it shows its robustness to scattered sharp areas in the background thanks to the powerful morphological simplification and the following region merging. Nonetheless, if the focused smooth region is too large, the proposed algorithm may need to incorporate some semantic or human knowledge. This algorithm can also be described as a recursive process of applying erosion operations to repeatedly reduce a set of points into smaller subsets using eight basic structuring elements. This is a natural generalization of the traditional skeleton transform. Each skeletal point from the new skeleton transform represents a shape element that is in general an octagon with four pairs of parallel opposing sides. Each pair of the opposing sides also has the same size.According to the experiments, the number of skeletal points used to represent a given shape is significantly lower than those used by the traditional skeleton transform, the MSD and the OMSD. The generalized skeleton transform easily leads to the construction of a new shape decomposition scheme, in which, a given shape is decomposed into a collection of modestly overlapping shape components, each of which is an octagon determined by the generalized skeleton transform. The main advantage of the new shape decomposition algorithm is that each shape component is represented by a single center point and the shape of a shape component is always primitive and explicitly specified using four integers. This allows easy comparison between two shape components. In future, this algorithm can be developed for object recognition from a low DOF image.

## REFERENCES

Besl, P.J. and R.C. Jain, 1988. Segmentation through variable-order surface fitting. IEEE. Trans. Pattern Anal. Mach. Intell. PAMO., 10: 167-192.

Comaniciu, D. and P. Meer, 1997. Robust analysis of feature spaces: Color image segmentation, In: Proc. IEEE. Conf. Computer Vision and Pattern Recognition, San Juaan, Puerto Rico, pp: 750-755.

Gonzalez, R.G. and R.E. Woods, 1992. Digital Image Processing. Reading, MA:Addison-Wesley.

Lifshitz, L.M. and S.M. Pizer, 1990. A multiresolution hierarchical approach to image segmentation based on intensity extrema, IEEE. Trans. Pattern Anal. Mach. Intell., 12: 529-540.

Tsai, D.M. and H.J. Wang, 1998. Segmenting focused onjects in complex visual images, Pattern Recognition Lett., 19: 929-949.

Won, C.S., K. Pyun and R.M. Gray, 2002. Automatic object segmentation in images with low depth of field, in Proc. Int. Conf. Image Processing, Rochester, NY, III: 805-808.

Wang, J.Z., J. Li, R.M. Gray and G. wiederhold, 2001. Unsupervised multiresolution segmentation for images with low depth of field, IEEE. Trans. Pattern Anal. Mach. Intell., 23: 85-90.

Yimand, C. and A.C. Bovik, 1998. Multiresolution 3-D range segmentation using focused cues, IEEE. Trans. Image Process., 7: 1283-1299.

Ye, Z. and C.C. Lu, 2002. Unsupervised multiscale focused objects detection using hidden Markov tree, in Proc. Int. Conf. Computer Vision, Pattern Recognition and Image Processing, Durham, NC., pp: 812-815.